JOURNAL OF SOLID STATE CHEMISTRY **121,** 291–300 (1996)
ARTICLE NO. 0040

Cationic Distribution in Two New Trivalent Transition Metal Diphosphates $Cd_5M_2^{III}(P_2O_7)_4$ (M = V, Fe)

S. Boudin, A. Grandin,[1] Ph. Labbé, D. Grebille, N. Nguyen, A. Ducouret, and B. Raveau

Laboratoire CRISMAT, ISMRA et Université de Caen, Bd du Maréchal Juin, 14050 Caen Cedex, France

Received April 21, 1995; in revised form September 20, 1995; accepted September 21, 1995

Two new diphosphates, $Cd_5M_2^{III}(P_2O_7)_4$ with M = V, Fe, isotypic with $Fe_5^{II}Fe_2^{III}(P_2O_7)_4$, have been synthesized. They crystallize in the space group $C222_1$ with $a \sim 8.8$ Å, $b \sim 9.9$ Å, and $c \sim 24.1$ Å. The single crystal structure determination of the V phase and the Mössbauer spectroscopy study of the Fe phase, show that the cationic distribution is different from that observed in $Fe_5^{II}Fe_2^{III}(P_2O_7)_4$, i.e., V(III) or Fe(III) is located in two kinds of sites instead of one kind of site. A detailed analysis of this structure shows that its octahedral layers consist of rock salt type ribbons, themselves built up from infinite chains of edge-sharing octahedra, interconnected through trioctahedral units of edge-sharing octahedra. On the basis of this description, the different cationic distribution compared to the pure Fe phase is then explained by the mismatch between infinite octahedral chains and trioctahedral units, due to the larger size of Cd(II) compared to Fe(II).

INTRODUCTION

The iron diphosphate $Fe_5^{II}Fe_2^{III}(P_2O_7)_4$, recently discovered by Genkina *et al.* (1) and B. Malaman *et al.* (2) is of great interest due to the mixed valent character of iron that is located in corner- and edge-sharing octahedra forming a rather close packed network. This original structure should imply a well-ordered distribution of the Fe(II) and Fe(III) species in the five octahedral independent sites of the structure. In fact the preliminary Mössbauer study suggests that this distribution is different from what could be expected from the Fe–O distances obtained by the XRD structure determination. The substitution of cadmium for iron in this phase confirms the particular cationic distribution in this structure. The diphosphate $Cd_{4.12}Fe_{0.88}^{II}Fe_2^{III}(P_2O_7)_4$, synthesized by Elbelghitti *et al.* (3), exhibits for one of the mixed ''Cd Fe'' sites an abnormally short M–O distance of 2.06 Å, if one takes into consideration the size of cadmium.

Trivalent vanadium, due to its size and to its ability to accommodate the octahedral coordination, exhibits a structural behavior similar to that of Fe(III), as shown for several diphosphates AMP_2O_7 with A = Na, K, Rb, Cs (4–13). In order to understand this particular behavior of the iron diphosphates $Fe_5^{II}Fe_2^{III}(P_2O_7)_4$, we have tried to substitute Cd and V(III) for iron in this compound. Thus, we report herein on the single crystal study of the new isotypic diphosphate $Cd_5V_2^{III}(P_2O_7)_4$ that exhibits mixed sites occupied by Cd(II) and V(III) simultaneously. This work is completed by the synthesis and Mössbauer study of the isostructural diphosphate $Cd_5Fe_2^{III}(P_2O_7)_4$, that contains only trivalent iron and is also curiously characterized by the existence of mixed ''CdFe'' sites.

CHEMICAL SYNTHESIS

Polycrystalline samples of the diphosphate $Cd_5V_2^{III}(P_2O_7)_4$ were prepared in two steps. First, a mixture of CdO, $H(NH_4)_2PO_4$, and V_2O_5 with the molar ratio Cd : V : P = 5 : 1.2 : 8 was heated to 673 K in air in order to eliminate NH_3 and H_2O. In a second step, the finely ground product with composition $Cd_5V_{1.2}P_8O_{28}$ was mixed with an appropriate amount of vanadium, placed in an alumina crucible, and sealed in an evacuated silica ampoule. The latter mixture was heated to 1225 K for 24 hr and quenched to room temperature.

Single crystals of $Cd_5V_2^{III}(P_2O_7)_4$ were isolated from a sample with the nominal composition $Cd_2V_4(PO_4)_6$. The synthesis was performed as described above with slow cooling to 1025 K with a rate of 1 K · hr^{-1} and furnace cooling to room temperature. The composition of the yellow crystals deduced from the structural determination was confirmed by microprobe analysis.

A polycrystalline sample of $Cd_5Fe_2^{III}(P_2O_7)_4$ was prepared by heating CdO, Fe_2O_3, and $H(NH_4)_2PO_4$ in air at 673 K, in stoichiometric ratio, to eliminate NH_3 and H_2O. The mixture was finely ground and heated to 1225 K under an oxygen pressure of 10 bars.

X-RAY DIFFRACTION STUDY OF $Cd_5M_2(P_2O_7)_4$ (M = Fe, V)

The powder X-ray diffraction patterns of the diphosphates $Cd_5V_2^{III}(P_2O_7)_4$ and $Cd_5Fe_2^{III}(P_2O_7)_4$ were registered

[1] To whom correspondence should be addressed.

0022-4596/96 $18.00

TABLE 1
Intereticular Distances (Å) in $Cd_5M_2^{III}(P_2O_7)_4$

h	k	l	d_{obs}	d_{calc}	I_{obs}
			$Cd_5V_2^{III}(P_2O_7)_2$		
0	0	2	12.019	12.019	37.4
1	1	1	6.3432	6.3432	24.2
0	0	4	6.0095	6.0095	2.4
1	1	2	5.7692	5.7691	21.2
1	1	3	5.0833	5.0835	30.5
0	2	0	4.9640	4.9643	4.4
0	2	1	4.8614	4.8617	20.8
0	2	2	4.5882	4.5882	17.1
1	1	4	4.4362	4.4362	1.1
2	0	0	4.3891	4.3891	1.8
2	0	1	4.3176	4.3176	8.8
0	2	3	4.2198	4.2200	7.0
0	0	6	4.0063	4.0063	8.3
1	1	5	3.8810	3.8810	17.8
0	2	4	3.8271	3.8273	14.9
0	2	5	3.4534	3.4535	7.8
1	1	6	3.4213	3.4215	10.9
2	2	0	3.2881	3.2882	7.1
2	2	1	3.2578	3.2578	27.0
2	2	2	3.1715	3.1717	89.1
0	2	6	3.1176	3.1177	3.77
1	3	0	3.0966	3.0967	33.0
1	3	1	3.0712	3.0713	40.0
1	1	7	3.0439	3.0440	6.2
2	2	3	3.0419	3.0420	63.7
0	0	8	3.0047	3.0047	100.0
1	3	2	2.9987	2.9988	3.6
2	0	6	2.9589	2.9590	1.2
1	3	3	2.8884	2.8885	3.6
2	2	4	2.8845	2.8846	12.1
0	2	7	2.8241	2.8241	5.5
3	1	1	2.7877	2.7877	2.7
1	3	4	2.7527	2.7528	1.8
3	1	2	2.7331	2.7332	18.9
1	1	8	2.7329	2.7330	8.1
2	2	5	2.7140	2.7141	26.3
2	0	7	2.7045	2.7045	3.9
3	1	3	2.6488	2.6489	26.0
1	3	5	2.6033	2.6034	1.0
3	1	4	2.5429	2.5430	12.1
2	2	6	2.5417	2.5417	19.7
0	4	0	2.4820	2.4821	1.3
2	0	8	2.4793	2.4794	4.0
1	1	9	2.4745	2.4745	1.2
1	3	6	2.4501	2.4501	5.3
0	4	2	2.4307	2.4308	4.8
3	1	5	2.4238	2.4239	11.8
2	2	7	2.3749	2.3750	3.5
0	4	3	2.3709	2.3709	4.6
0	2	9	2.3520	2.3520	4.9
1	3	7	2.2997	2.2997	6.8
3	1	6	2.2987	2.2987	2.1
0	4	4	2.2941	2.2941	15.3
2	0	9	2.2816	2.2816	1.4

TABLE 1—*Continued*

h	k	l	d_{obs}	d_{calc}	I_{obs}
			$Cd_5V_2^{III}(P_2O_7)_2$		
0	0	2	11.998	12.000	24.1
1	1	1	6.3329	6.3347	18.5
0	0	4	5.9989	5.9997	3.0
1	1	2	5.7595	5.7610	15.5
1	1	3	5.0749	5.0760	25.0
0	2	0	4.9594	4.9610	2.9
0	2	1	4.8567	4.8583	14.2
0	2	2	4.5833	4.5847	13.0
2	0	0	4.3796	4.3809	1.3
2	0	1	4.3085	4.3096	7.6
0	2	3	4.2148	4.2160	5.3
0	0	6	3.9991	3.9999	7.7
1	1	5	3.8743	3.8752	15.7
2	0	3	3.8415	3.8423	1.4
0	2	4	3.8222	3.8234	12.7
0	2	5	3.4487	3.4496	8.6
1	1	6	3.4155	3.4162	10.6
2	2	0	3.2828	3.2838	8.7
2	2	1	3.2525	3.2535	17.4
2	2	2	3.1665	3.1673	75.0
0	2	6	3.1131	3.1138	9.1
1	3	0	3.0932	3.0942	26.9
1	3	1	3.0678	3.0689	32.7
1	1	7	3.0387	3.0393	7.5
2	2	3	3.0370	3.0378	52.8
0	0	8	2.9994	3.0000	100.0
1	3	2	2.9953	2.9962	3.8
2	0	6	2.9532	2.9539	5.2
1	3	3	2.8850	2.8859	6.0
2	2	4	2.8798	2.8805	13.0
0	2	7	2.8199	2.8205	3.6
3	1	1	2.7821	2.7828	2.3
1	3	4	2.7493	2.7500	2.3
1	1	8	2.7282	2.7287	5.5
3	1	2	2.7276	2.7283	15.7
2	2	5	2.7095	2.7926	19.9
2	0	7	2.6994	2.7000	5.1
3	1	3	2.6436	2.6442	20.8
1	3	5	2.6000	2.6007	1.3
3	1	4	2.5379	2.5386	10.0
2	2	6	2.5374	2.5380	16.1
1	1	9	2.4703	2.4707	3.9
1	3	6	2.4468	2.4474	4.1
0	4	2	2.4284	2.4292	4.1
3	1	5	2.4191	2.4197	10.2
2	2	7	2.3709	2.3715	3.9
0	4	3	2.3685	2.3692	4.0
0	2	9	2.3483	2.3488	3.1
1	3	7	2.2965	2.2970	6.5
3	1	6	2.2942	2.2948	2.6
0	4	4	2.2916	2.2923	8.8
2	0	9	2.2773	2.2778	1.9
1	1	10	2.2537	2.2542	3.6

TABLE 2
Cell Parameters of $M_5^{II}M_2'^{III}(P_2O_7)_4$ Structures

$M_5^{II}M_2'^{III}$	$Fe_5^{II}Fe_2^{III}$	$Cd_{4.12}^{II}Fe_{0.88}^{II}Fe_2^{III}$	$Cd_5^{II}Fe_2^{III}$	$Cd_5^{II}V_2^{III}$
a (Å)	8.451 (1)[a] 8.4327 (7)[b]	8.702 (1)	8.715 (6)	8.7780 (7)
b	9.691 (1)[a] 9.695 (1)[b]	9.889 (1)	9.9217 (7)	9.9282 (8)
c	23.626 (5)[a] 23.663 (4)[b]	23.968 (3)	23.999 (1)	24.037 (2)
V(Å^3)	1934.9 (9)[a] 1934[b]	2062.5 (3)	2086 (2)	2094.5 (6)

[a] Reference (1).
[b] Reference (2).

on a Philips diffractometer with Cu$K\alpha$ radiation. Both spectra were indexed in an orthorhombic cell as shown for the V(III) diphosphate (Table 1). The cell parameters of these phases, compared to those of $Cd_{4.12}Fe_{0.88}^{II}Fe_2^{III}(P_2O_7)_4$ (3) and of $Fe_5^{II}Fe_2^{III}(P_2O_7)_4$ (1–2) (Table 2), show that the Cd phases exhibit larger parameters than the Fe(II) diphosphates due to the larger size of cadmium; similarly the V(III) diphosphate $Cd_5V_2^{III}(P_2O_7)_4$ has larger parameters than the Fe(III) diphosphate $Cd_5Fe_2^{III}(P_2O_7)_4$, in agreement with the relative sizes of V(III) and Fe(III).

A yellow crystal of $Cd_5V_2^{III}(P_2O_7)_4$ with the dimensions $0.039 \times 0.051 \times 0.077$ mm was selected for the X-ray diffraction study on a Enraf Nonius CAD4 diffractometer, using Mo$K\alpha$ radiation with a graphite monochromator. The orthorhombic cell parameters (Table 3) were determinated and refined using 25 reflections with $18° < \theta < 22°$

TABLE 3
Summary of Crystal Data Intensity Measurements and Structure Refinement Parameters for $Cd_5V_2^{III}(P_2O_7)_4$

Crystal data	
Space group	$C222_1$
Cell dimensions	a = 8.7659(5) Å b = 9.9267(9) Å c = 24.045(2) Å
Volume	2092.3(5) Å^3
Z	4
ρ_{calc} (g cm^{-3})	4.32
Intensity measurements	
λ (Mo$K\alpha$)	0.71073 Å
Scan mode	$\omega - 5/3\ \theta$
Scan width (°)	1.1 + 0.35 tan θ
Slit aperture (mm)	1.06 + tan θ
Max (θ (°))	45
Standard reflections	3 measured every 3000 sec
Range	
h	$0 \rightarrow 17$
k	$0 \rightarrow 19$
l	$0 \rightarrow 47$
Measured reflections	4727
Reflections with $I > 3\ \sigma$	930
μ (mm^{-1})	7.07
Structure solution and refinement	
Parameters refined	127
Agreement factors	R = 0.037 Rw = 0.038
Weighting scheme	$w = F(\sin\theta/\lambda)$
Δ/σ max	< 0.004
$\Delta\rho$ (e/Å^3)	0.8

TABLE 4
Positional Parameters and Their Estimated Standard Deviations

Atom	x	y	z	B_{eq}/B(Å^2)
M(1) = Cd(1)	0.1912(2)	0	0.5	0.73(2)
M(2) = Cd(2)	0.5816(2)	0	0.5	0.99(3)
M(3) = Cd(3)	0.8133(2)	0.6496(1)	0.13532(5)	0.83(2)
M(4) = 80% V + 20% Cd	0.0746(2)	0.1600(2)	0.37734(9)	0.67(3)
M(5) = 40% V + 60% Cd	0	0.2005(3)	0.75	0.83(4)
P(1)	0.5977(5)	0.2965(4)	−0.0043(2)	0.62(6)
P(2)	0.3879(6)	0.3660(4)	0.3835(2)	0.66(6)
P(3)	0.1228(5)	0.4523(4)	0.1253(2)	0.53(6)
P(4)	0.2452(6)	0.0501(5)	0.2689(2)	0.78(7)
O(1)	0.2280(1)	−0.001(1)	0.4003(5)	0.7(2)*
O(2)	0.039(1)	0.160(1)	0.4609(5)	0.8(2)*
O(3)	−0.113(1)	0.296(1)	0.3709(5)	0.7(2)*
O(4)	0.230(2)	0.307(1)	0.3859(5)	1.2(2)*
O(5)	0.123(2)	0.129(1)	0.3009(5)	1.4(2)*
O(6)	−0.105(1)	0.016(1)	0.3737(5)	1.0(2)*
O(7)	0.002(2)	0.203(1)	0.8445(5)	1.1(2)*
O(8)	0.184(2)	0.071(1)	0.7575(6)	2.2(3)*
O(9)	0.169(2)	0.359(1)	0.7286(5)	1.5(2)*
O(10)	0.614(1)	0.145(1)	−0.0015(5)	0.6(1)*
O(11)	0.748(1)	0.357(1)	−0.0245(5)	1.2(2)*
O(12)	0.547(1)	0.352(1)	0.0548(5)	1.0(2)*
O(13)	−0.015(1)	0.513(1)	0.0980(5)	0.9(2)*
O(14)	0.121(2)	0.509(1)	0.1877(5)	1.0(2)*

Note. Starred atoms were refined isotropically. Anisotropically refined atoms are given in the form of the isotropic equivalent displacement parameter defined as $B_{eq} = 4/3\ [\beta_{11}a^{*2} + \beta_{22}b^{*2} + \beta_{33}c^{*2} + \beta_{12}a^* \cdot b^* \cos\gamma^* + \beta_{13}a^*b^* \cos\beta^* + \beta_{23}b^* \cdot c^* \cdot \cos\alpha^*]$.

at 294 K. The data collection containing 930 reflections, with $I > 3\sigma(I)$, out of 4727 were considered for the structural resolution. The systematic extinctions $h + k = 2n + 1$ for all $h\ k\ l$, ($h = 2n + 1$) for $h\ 0\ l$, ($k = 2n + 1$) for $0\ k\ l$, ($h = 2n + 1$) for $h\ 0\ 0$, ($k = 2n + 1$) for $0\ k\ 0$, and $l = 2n + 1$ for $0\ 0\ l$ were consistent with the space group $C222_1$ (no. 20). The intensities were corrected from the Lorentz and polarization effects. The structure resolution, using a heavy atom method and a least-squares refinement with SDP programs (14) leads to the atomic parameters reported in Table 4. Note that the anisotropic thermal factors were not calculated for the oxygen atoms. No absorption correction due to the small size of the crystal was applied, but secondary effect extinction correction was performed leading to $R = 0.037$ and $R_w = 0.038$.

DISCUSSION OF THE $Cd_5V_2(P_2O_7)_4$ STRUCTURE

The structure of $Cd_5V_2^{III}(P_2O_7)_4$ is very similar to that previously described for $Fe_5^{II}Fe_2^{III}(P_2O_7)_4$ (1–2). The projec-

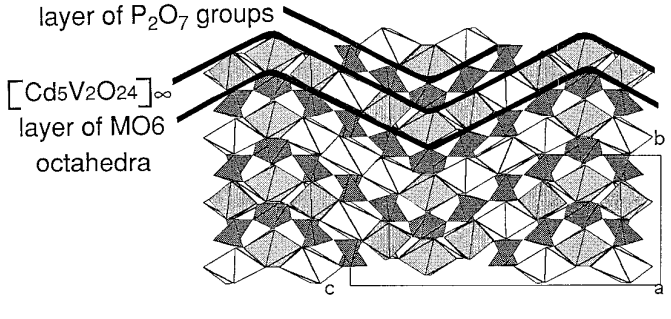

FIG. 1. Projection of the $Cd_5V_2^{III}(P_2O_7)_4$ structure along **a**.

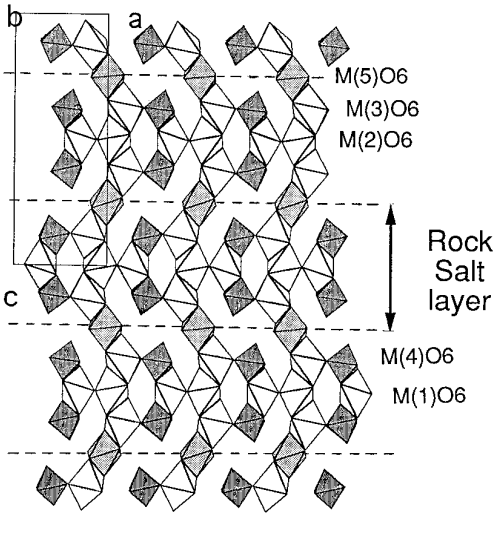

FIG. 2. Projection of one $[Cd_5V_2O_{24}]_\infty$ layer along **b**.

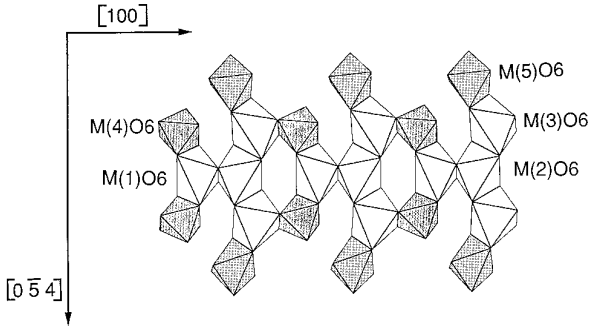

FIG. 3. Rock salt-type ribbon parallel to $(0\,4\,5)_o$, i.e., $(1\,1\,1)_c$ ($_c$ for conventional cubic cell of rock salt).

tion of the structure along **a** (Fig. 1) shows that it consists of undulating octahedral layers of edge-sharing CdO_6 and VO_6 octahedra interconnected through discontinuous layers of diphosphate groups. The tridimensionnal framework is constructed by stacking one octahedral layer with one tetrahedral layer along **b** alternately. The corrugated $[Cd_5V_2O_{24}]_\infty$ layers whose mean plane is parallel to (010) (Fig. 2) are built up from chains of edge-sharing VO_6 and CdO_6 octahedra waving along **c**, interconnected along **a** through units of three edge-sharing octahedra. The trioctahedral units and the infinite octahedral chains share edges forming distorted hexagonal rings. At this stage, a deeper analysis of the geometry of these octahedral layers is necessary. It shows that the waving $[Cd_5V_2O_{24}]_\infty$ layers are built up from distorted, vacated, rock salt type ribbons running along **a** and that are at maximum five octahedra wide along **c** (Fig. 3). Two successive rock salt type ribbon share the edges of their octahedra along **c** (Fig. 2) and have their plane parallel to $(111)_c$ an $(1\bar{1}1)_c$ respectively, i.e., are roughly parallel to the $[045]_o$ and $[04\bar{5}]_o$ directions of the orthorhombic cell alternately. In fact, each rock salt ribbon consists of two kinds of octahedral strings that are five and three octahedra long along **c** alternately (Fig. 2).

The great originality of this structure deals with the

TABLE 5
Bond Distances (Å) and Angles (°) in the MO_6 and PO_4 Polyhedra

M(4) (80% V + 20% Cd)	O(1)	O(2)	O(3)	O(4)	O(5)	O(6)
O(1)	**2.17 (1)**	2.73 (2)	4.27 (2)	3.08 (2)	2.87 (2)	3.00 (2)
O(2)	81.0 (5)	**2.03 (1)**	2.88 (2)	2.87 (2)	3.93 (2)	2.83 (2)
O(3)	165.0 (4)	87.3 (5)	**2.14 (1)**	3.04 (2)	3.10 (2)	2.78 (2)
O(4)	95.1 (5)	90.3 (5)	94.2 (5)	**2.01 (1)**	2.86 (2)	4.13 (2)
O(5)	89.3 (5)	169.7 (6)	101.8 (5)	93.7 (6)	**1.91 (1)**	2.88 (2)
O(6)	88.6 (5)	85.7 (5)	81.3 (5)	174.1 (5)	91.0 (5)	**2.12 (1)**
M(5) (40% V + 60% Cd)	O(7)	O(7^{i})	O(8)	O(8^{i})	O(9)	O(9^{i})
O(7)	**2.27 (1)**	4.55 (2)	2.94 (2)	3.22 (2)	3.51 (2)	2.78 (2)
O(7^{i})	178.3 (5)	**2.27 (1)**	3.22 (2)	2.94 (2)	2.78 (0)	3.51 (2)
O(8)	85.0 (5)	95.7 (5)	**2.07 (2)**	3.24 (2)	2.95 (2)	4.22 (2)
O(8^{i})	95.7 (5)	85.0 (5)	103.1 (6)	**2.07 (2)**	4.22 (2)	2.95 (2)
O(9)	102.7 (5)	76.5 (5)	86.7 (6)	159.9 (5)	**2.22 (1)**	3.13 (2)
O(9^{i})	76.5 (5)	102.7 (5)	159.9 (5)	86.7 (6)	89.7 (5)	**2.22 (1)**
P(1)	O(2^{ii})	O(10)	O(11)	O(12)		
O(2^{ii})	**1.52 (1)**	2.53 (2)	2.54 (2)	2.38 (2)		
O(10)	112.5 (7)	**1.52 (1)**	2.47 (2)	2.53 (2)		
O(11)	112.9 (7)	108.8 (7)	**1.52 (1)**	2.59 (2)		
O(12)	100.1 (7)	109.3 (7)	113.0 (7)	**1.59 (1)**		
P(2)	O(4)	O(6^{iii})	O(7^{ii})	O(12)		
O(4)	**1.50 (1)**	2.55 (2)	2.55 (2)	2.46 (2)		
O(6^{iii})	115.4 (8)	**1.51 (1)**	2.46 (2)	2.42 (2)		
O(7^{ii})	115.9 (8)	108.9 (7)	**1.51 (1)**	2.51 (2)		
O(12)	104.9 (7)	102.5 (7)	108.1 (7)	**1.59 (1)**		
P(3)	O(1^{v})	O(3^{vi})	O(13)	O(14)		
O(1^{v})	**1.51 (1)**	2.54 (2)	2.52 (2)	2.50 (2)		
O(3^{vi})	111.8 (7)	**1.56 (1)**	2.54 (2)	2.55 (2)		
O(13)	113.2 (7)	112.5 (7)	**1.50 (1)**	2.46 (2)		
O(14)	106.4 (7)	107.2 (7)	105.1 (7)	**1.60 (1)**		

TABLE 5—*Continued*

$M(4)$ (80% V + 20% Cd)	O(1)	O(2)	O(3)	O(4)	O(5)	O(6)
P(4)	O(5)	O(8^{vii})	O(9^{ii})	O(14^{viii})		
O(5)	**1.53 (1)**	2.49 (2)	2.52 (2)	2.55 (2)		
O(8^{vii})	112.4 (9)	**1.46 (1)**	2.49 (2)	2.53 (2)		
O(9^{ii})	111.3 (9)	113.1 (8)	**1.52 (1)**	2.44 (2)		
O(14^{viii})	108.0 (8)	109.9 (8)	101.5 (7)	**1.62 (1)**		

Cd(1)–O(1)	2.42 (1)	Cd(2)–O(10^{ix})	2.24 (1)
Cd(1)–O(1^{vii})	2.42 (1)	Cd(2)–O(10^{iv})	2.24 (1)
Cd(1)–O(2)	2.28 (1)	Cd(2)–O(11^{x})	2.15 (1)
Cd(1)–O(2^{vii})	2.28 (1)	Cd(2)–O(11^{xi})	2.15 (1)
Cd(1)–O(10^{ix})	2.23 (1)	Cd(2)–O(13^{xii})	2.43 (1)
Cd(1)–O(10^{iv})	2.23 (1)	Cd(2)–O(13^{viii})	2.43 (1)
Cd(3)–O(3^{v})	2.28 (1)		
Cd(3)–O(7^{xiii})	2.26 (1)		
Cd(3)–O(9^{xiv})	2.25 (1)		
Cd(3)–O(11^{xv})	2.73 (1)		
Cd(3)–O(13^{xvi})	2.22 (1)		
Cd(3)–O(6^{v})	2.27 (1)		

Symmetry codes

i	$-x$	y	$-z + 3/2$
ii	$-x + 1/2$	$-y + 1/2$	$z - 1/2$
iii	$x + 1/2$	$y + 1/2$	z
iv	$-x + 1$	y	$-z + 1/2$
v	$-x + 1/2$	$y + 1/2$	$-z + 1/2$
vi	$-x$	y	$-z + 1/2$
vii	x	$-y$	$-z + 1$
viii	$-x + 1/2$	$y - 1/2$	$-z + 1/2$
ix	$-x + 1$	$-y$	$z + 1/2$
x	$-x + 3/2$	$-y + 1/2$	$z + 1/2$
xi	$-x + 3/2$	$y - 1/2$	$-z + 1/2$
xii	$-x + 1/2$	$-y + 1/2$	$z + 1/2$
xiii	$x + 1$	$-y + 1$	$-z + 1$
xiv	$-x + 1$	$-y + 1$	$z - 1/2$
xv	x	$-y + 1$	$-z$
xvi	$x + 1$	y	z

simultaneous occupancy of the octahedral sites of the rock salt ribbons by vanadium and cadmium, in spite of the significantly different size of V(III) and Cd(II). The octahedral sites located inside the ribbons (labeled $M(1)$, $M(2)$ and $M(3)$ in Figs. 2 and 3) are all fully occupied by cadmium, with Cd–O distances ranging from 2.15 to 2.73 Å, in agreement with those usually observed for this element in octahedral coordination. The two other sites, $M(4)$ and $M(5)$, located at the extremities of the strings exhibit a mixed occupancy by cadmium and vanadium. The rate of each atom, on each site, was first roughly determined from the intermediate electronic density, observed on $M(4)$ and $M(5)$ sites, and then was refined, leading to 0.8 V + 0.20 Cd on $M(4)$ site and 0.60 Cd + 0.40 V on $M(5)$ site. Variations of ± 5% of these rates was tested but give worse agreement with the thermal agitation parameters and with the R factors. The smaller $M(4)$ site, which is located at the ends of the trioctahedral units (Figs. 2 and 3) is mainly occupied by vanadium (80%), in agreement with its smaller size. The interatomic distances corresponding to the O(4) and O(5) atoms of this site (2.01 and 1.91 Å, Table 4) are abnormally small to be compatible with Cd–O distances; it is most probable that, locally, the oxygen atoms surrounding cadmium deviate from these positions, especially for O(5), in agreement with its higher B factor. Anistropic thermal refinement of oxygen atoms should have shed some light in this issue but unfortunately would not be significant here due to the too large number of variable parameters. The $M(5)$ site, located at the boundary between two rock salt ribbons (Figs. 2 and 3), is preferentially occupied by cadmium (60%); $M(4)$–O distances, ranging from 2.07 to 2.27 Å (Table 5) are compatible with the

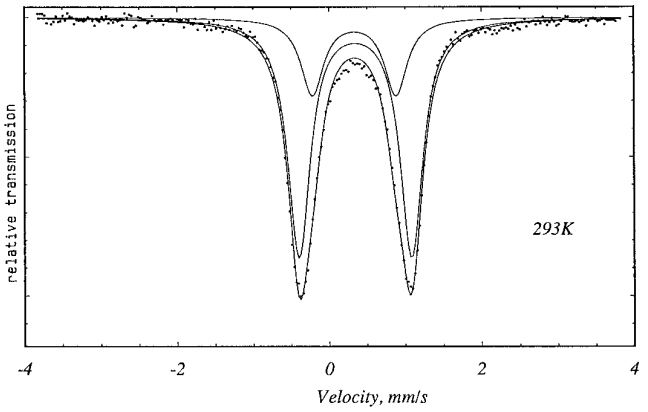

FIG. 4. ^{57}Fe Mössbauer absorption powder spectrum of $Cd_5Fe_2^{III}(P_2O_7)_4$.

presence of cadmium and trivalent vanadium, especially if we take into account the higher B factor of O(8) (2.2 Å^2), which suggests a possible splitting of this atomic position. The enantiomorphic structure has been tested without significant different results.

These results show the ability of V(III) and Cd(II) to form rock salt ribbons in spite of their different size. An important issue deals with the distribution of the cationic species over the different octahedral sites. One would indeed expect a complete ordering of V(III) and Cd(II), leading to infinite rows of edge-sharing octahedra running along **c**, completely occupied by cadmium ($M(2)$, $M(3)$, $M(5)$ sites), whereas the $M(4)$ sites of the trioctahedral units would be completely occupied by vanadium. Such an ordering may introduce too large strains between the infinite octahedral chains and the trioctahedral units, due to a large mismatch between the latter. This explains the partial disordering of cadmium and vanadium between the $M(4)$ and $M(5)$ sites which would reduce this mismatch between the infinite chains and the trioctahedral units. If such a hypothesis is exact, the phosphate $Cd_5Fe_2^{III}(P_2O_7)_4$, if it exists, should also exhibit two kinds of sites for trivalent iron. For this reason, we tried to synthesize this compound. Iron phosphate was obtained as a pure phase, in the form of a polycrystalline sample, with parameters very similar to those of $Cd_5V_2^{III}(P_2O_7)_4$ (Table 2), in agreement with the relative sizes of V(III) and Fe(III). In order to understand the distribution of trivalent iron in the latter structure, a Mössbauer study was carried out.

TABLE 6
Fitted Mössbauer Parameters of $Cd_5Fe_2^{III}(P_2O_7)_4$ at 293 K

Site	IS ± 0.01[a] (mm/sec)	Γ ± 0.02[b] (mm/sec)	|QS| ± 0.02[c] (mm/sec)	% ± 5[d]
1	0.45	0.35	1.48	74
2	0.44	0.35	1.10	26

[a] IS: isomer shift relative to metallic iron at room temperature.
[b] Γ: half height width.
[c] QS: quadrupole splitting.
[d] %: fitted relative intensity.

MÖSSBAUER SPECTROSCOPY AND ELECTRIC FIELD GRADIENT CALCULATIONS OF $Cd_5Fe_2^{III}(P_2O_7)_4$

The Mössbauer spectrum of ^{57}Fe was registered in a transmission geometry with a constant acceleration spectrometer using a ^{57}Co source in a Rh matrix. It was fitted using the MOSFIT program (15).

A Mössbauer absorption powder spectrum of $Cd_5Fe_2^{III}(P_2O_7)_4$ was recorded at room temperature (Fig. 4). It indicates the presence of pure electronic quadrupolar interactions, and can be analyzed with two quadrupole components (Table 6). The observed isomer shift (IS) values are characteristic of trivalent iron and the absolute values of the quadrupole splitting (QS) (1.48 and 1.10 mm/sec) are similar to that previously found for Fe(III) in the $Fe_5^{II}Fe_2^{III}(P_2O_7)_2$ compound (IS ≈ 0.4 mm/sec; QS ≈ 1.2 mm/sec) (1–2).

Because it was not possible to isolate any single crystals from the sample of nominal composition $Cd_5Fe_2^{III}(P_2O_7)_4$, we could not perform a correct structural study to determine the iron distribution in the five different crystallographic M_i sites. However, according to the above structural results of the homologous vanadium $Cd_5V_2^{III}(P_2O_7)_4$ compound and to the similar size of Fe(III) and V(III) ions, one can suppose that Fe(III) ions are also located in the $M(4)$ and $M(5)$ sites like V(III) ions.

In order to propose a logical correspondance between these $M(4)$ and $M(5)$ sites and the two experimental Mössbauer components which have quite different QS values, electric field gradient (EFG) calculations have been performed.

The quadrupole splitting, observed in the Mössbauer

TABLE 7
Comparison Between Monopolar Calculated and Experimental Mössbauer Quadrupole Splitting QS Values

	$Cd_5Fe_2^{III}(P_2O_7)_4$		$Fe_5^{II}Fe_2^{III}(P_2O_7)_4$
EFG results	$M(4)$ (8c)	$M(5)$ (4a)	$M(4)$ (8c)
V_{ZZ} (mm/sec)	0.75	−0.51	0.82
η	0.85	0.29	0.42
QS (monopolar) (mm/sec)	0.83	−0.52	0.84
Mössbauer analysis	Site 1	Site 2	Fe^{III}
|QS| (mm/sec)	1.48	1.10	1.22
|QS| (dipol)	0.65	0.58	0.38

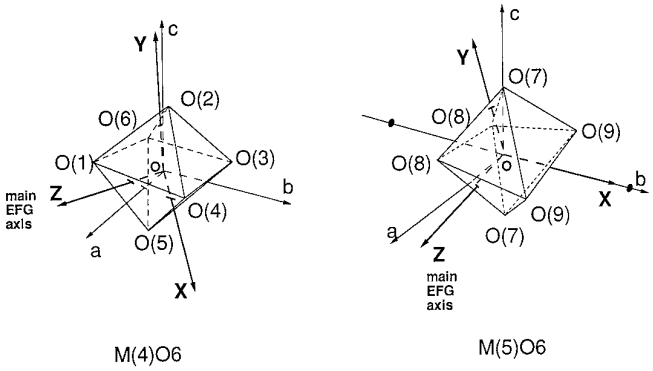

FIG. 5. $M(4)O_6$ (left) and $M(5)O_6$ (right) octahedra in the main axes (O**X**, O**Y**, O**Z**) of the EFG tensor and in the translated (**a**, **b**, **c**) cristallographic axes.

spectra, corresponds to the asymmetrical part of the electric hyperfine interaction between the iron nucleus and its surrounding charges (electrons from the iron valence shell and other ions in the crystal).

Due to the spherical symmetry of the $3d^5$ electronic shell of Fe^{3+}, no "valence contribution" occurs in the EFG tensor $[V_{ij}]$ of this ion.

The EFG is only due to the "lattice" contribution.

Consequently, QS values can be deduced from the main components V_{XX}, V_{YY}, V_{ZZ} of the EFG tensor by the relation

$$QS = (1 - \gamma_\infty)\frac{eQ}{2}V_{ZZ}\left(1 + \frac{\eta^2}{3}\right)^{1/2}$$

where $(1 - \gamma_\infty)$ is the antishielding Sternheimer factor ($\sim$10.14 for Fe^{3+}) (16), V_{ZZ} is the principal component of the EFG tensor, $\eta = (V_{XX}\text{-}V_{YY})/V_{ZZ}$ is the asymmetry parameter ($0 \le \eta \le 1$, with the convention $|V_{XX}| \le |V_{YY}| \le |V_{ZZ}|$), and Q is the quadrupolar moment of the ^{57}Fe nucleus in the excited state $I = 3/2$ ($Q \sim 0.2$ barn (17)).

We have thus computed lattice EFG calculations for Fe(III) in the $M(4)$ and $M(5)$ sites of the structure successively.

Though QS results from the summation of decreasing multipolar contributions (QS = QS (monopol) + QS (dipol) + ...), in this work we have only considered the monopolar approximation (charge point model), but use the whole crystal (instead of the first neighbors only).

As the cell parameters of the Fe(III) and V(III) phases are nearly similar, the monopolar EGF calculations have been performed using the parameters and atomic positions corresponding to the vanadium phase (Table 7). Therefore, the results must be considered only as qualitative indications to compare the Fe(III) environment in $M(4)$ and $M(5)$ sites.

Moreover, in order to have an approach with the homologous $Fe_5^{II}Fe_2^{III}(P_2O_7)_4$ compound, we have also performed similar EFG calculations for the Fe(III) ions located in the $M(4)$ site of this phase, in which the atomic positions are clearly established by a structural study (1). Computed values of V_{ZZ}, η, and QS are given in Table 7.

For the $Cd_5Fe_2^{III}(P_2O_7)_4$ phase, a positive EFG gradient is obtained in the case of Fe(III) in the $M(4)$ site, with a main O**Z** axis near by the crystallographic $[1\bar{1}0]$, O**Y** lying near by the **c** axis (Fig. 5). The asymmetry parameter ($\eta = 0.85$) is rather high.

A lower, but negative value of V_{ZZ} is observed for Fe(III) in the $M(5)$ site, with O**Z** in the (**a**, **c**) plane (at about 14° from the **a** axis) and O**X** lying along the twofold **b** axis. A lower η value is also obtained ($\eta = 0.29$).

These results evidence a more symmetrical local environment of iron in the $M(5)$ site than in the $M(4)$ one, as it can be seen also from the comparison between the absolute values of the calculated QS (0.83 and 0.52 mm/sec, respectively) for the $M(4)$ and $M(5)$ sites. This allows us to attribute the $M(4)$ site to the Mössbauer site 1 ($|QS| = 1.48$ mm/sec) whereas the $M(5)$ site corresponds to the Mössbauer site 2 ($|QS| = 1.10$ mm/sec).

Calculations correctly reproduce the $|QS|$ difference between the two sites $|QS|_{M4} - |QS|_{M5} \sim 0.31$ mm/sec compared to $|QS|_1 - |QS|_2 \sim 0.38$ mm/sec).

The $M(4)$ calculated results are consistent with those obtained for Fe(III) in the same site of the $Fe_5^{II}Fe_2^{III}(P_2O_7)_4$ compound (Table 7). Note that, for this latter phase, though the EFG calculations have been performed using more realistic atomic positions, there remains some difference (0.38 mm/sec) between the calculated $|QS|$ value and the experimental one, as for the $M(4)$ and $M(5)$ sites of the mixed Cd–Fe compound (0.65 and 0.58 mm/sec, respectively). Therefore, this difference could be mainly attributed to the neglected dipolar (and multipolar) contributions to the iron EFG tensor, coming from the distorted electronic clouds around the different ions of the crystal.

Calculations of such dipolar effects would need a complete knowledge of the $[\alpha]$ polarizability tensors on each ion and would require a self consistent process, very expensive in time and memory size, to determine electric fields and gradients, due to the great number of atoms (172) in the elementary cell. So, these calculations have not been performed here, but the comparison between monopolar results and experimental results shows that the dipolar contribution (0.4–0.6 mm/sec) is not negligible in these compounds where the oxygen polarizabilities are probably the most relevant factors.

For the $Cd_5Fe_2^{III}(P_2O_7)_4$ phase, it can be noted that, as for the monopolar term, the dipolar part of QS is slightly smaller for the more symmetric $M(5)$ site than for the $M(4)$ site. Otherwise, the line intensities observed for the Mössbauer site 1 (75%) and site 2 (25%) agree with the tendency of the iron ions to be located in the site of smaller

size. This consideration is coherent with the site attribution by EFG calculations, in which 75% of Fe(III) lies in the smallest and less symmetrical $M(4)$ site. Thus, the Fe(III)/Cd(II) ratios of 75:25% in $M(4)$ and 50:50% in $M(5)$ sites, are very close to the V(III)/Cd(II) ratios observed for $Cd_5V_2^{III}(P_2O_7)_4$ (80:20% and 40:60%, respectively).

CONCLUDING REMARKS

A V(III) diphosphate, involving rock salt type ribbons built up from CdO_6 and VO_6 octahedra has been synthesized for the first time. The ability of V(III) to coexist with Cd(II) in these rock salt ribbons is remarkable. This feature is also observed for Fe(III) in the isostructural diphosphates $Cd_5Fe_2^{III}(P_2O_7)_4$, $Fe_5^{II}Fe_2^{III}(P_2O_7)_4$ (1–2), and $Cd_{4.12}Fe_{0.88}^{II}Fe_2^{III}(P_2O_7)_4$ (3) in agreement with the similar behavior of Fe(III) and V(III). Nevertheless, one observes a significantly different distribution of the cationic species in the diphosphate containing Fe(II).

In $Fe_5^{II}Fe_2^{III}(P_2O_7)_4$ (1–2) and $Cd_{4.12}Fe_{0.88}^{II}Fe_2^{III}(P_2O_7)_4$ (3) the Fe(III) species lies only in one kind of site, $M(4)$, so that the structure consists of infinite chains of CdO_6 and/or $Fe^{II}O_6$ octahedra running along **c**, interconnected through trioctahedral units built up of two Fe(III) and one Fe(II). In contrast, in $Cd_5V_2^{III}(P_2O_7)_4$ and $Cd_5Fe_2(P_2O_7)_4$ the Fe(III) or V(III) species are distributed over two kinds of sites, $M(4)$ and $M(5)$, i.e., in both infinite chains and trioctahedral units simultaneously. This difference can be explained by the size of Cd(II), significantly larger than that of Fe(II); a partial or complete ordered replacement of Fe(II) by Cd(II) in the $M(5)$ sites of the infinite octahedral chains increases the size difference, and consequently the mismatch between the chain and the trioctahedral units. Consequently, a partial disordering between Cd(II) and Fe(III) of V(III) is necessary in the cadmium rich phases Cd_5 to ensure the stability of the structure.

REFERENCES

1. E. A. Genkina, B. A. Maksimov, O. V. Zvereva, Yu. M. Mininzon, I. S. Lyubutin, S. V. Luchko, and V. V. Yakovlev, *Sov. Phys. Crystallogr.* **37,** 627 (1992).
2. B. Malaman, M. Ijlaali, R. Gerardin, G. Venturini, and C. Gleitzer, *Eur. J. Solid State Inorg. Chem.* **29,** 1269 (1992).
3. A. Elbelghitti and A. Boukhari, *Acta Crystallogr. Sect. C* **50,** 1648 (1994).
4. D. Riou, N. Nguyen, R. Benloucif, and B. Raveau, *Mater. Res. Bull.* **25,** 1363 (1990).
5. K. H. Lii, Y. P. Wang, Y. B. Chen, and S. L. Wang, *J. Solid State Chem.* **86,** 143 (1990).
6. T. Moya-Pizarro, R. Salmon, L. Fournes, G. Le Flem, B. Wanklyn, and P. Hagenmuller, *J. Solid State Chem.* **53,** 387 (1984).
7. Y. P. Wang, K. H. Lii and S. L. Wang, *Acta Crystallogr. Sect. C* **45,** 1417 (1989).
8. D. Riou, Ph. Labbé, and M. Goreaud, *Eur. J. Solid State Inorg. Chem.* **25,** 215 (1988).
9. L. Benhamada, A. Grandin, M. M. Borel, A. Leclaire, and B. Raveau, *Acta Crystallogr. Sect. C* **47,** 424 (1991).
10. J. M. M. Millet and B. F. Mentzen, *Eur. J. Solid State Chem.* **28,** 493 (1991).
11. U. Flörke, *Z. Kristallog.* **191,** 137 (1990).
12. E. Dvoncova and K. H. Lii, *J. Solid State Chem.* **105,** 279 (1993).
13. Y. P. Wang and K. H. Lii, *Acta Crystallogr. Sect. C* **45,** 1210 (1989).
14. B. A. Frenz and Associates, Inc., ''SDP Structure Determination Package.'' College Station, Texas, 1982.
15. J. Teillet and F. Varret, unpublished MOSFIT program.
16. R. M. Sternheimer, *Phys. Rev.* **130,** 1423 (1963).
17. P. Gütlich, R. Link, and A. Trautwein, ''Inorganic Chemistry Concepts, Vol. 3, Mössbauer Spectroscopy and Transition Metal Chemistry.'' Springer-Verlag, Berlin, 1978.